




## Letter

Signature of  $0^+$  excited state and shape coexistence in  $^{94}\text{Kr}$  through  $^{93}\text{Kr}(d,p)^{94}\text{Kr}$  reaction

D. Walter<sup>a,b</sup>, R. Kanungo<sup>a,b, \*</sup>, M. Holl<sup>a,b</sup>, S. Roy-Garand<sup>a</sup>, B.S. Hu<sup>b</sup>, J.D. Holt<sup>b</sup>, M. Alcorta<sup>b</sup>, C. Andreoiu<sup>c</sup>, S. Bhattacharjee<sup>b</sup>, A.A. Chen<sup>e</sup>, A. Chester<sup>b</sup>, D. Connolly<sup>b</sup>, B. Davids<sup>b,d</sup>, N. Esker<sup>b</sup>, F. Garcia<sup>c</sup>, S. Gillespie<sup>b</sup>, G. Hackman<sup>b</sup>, S. Ishimoto<sup>f</sup>, R. Krücken<sup>b,g</sup>, P. Jassal<sup>a</sup>, J. Laroche<sup>a</sup>, J. Liang<sup>e</sup>, B. Olaizola<sup>b</sup>, A. Psaltis<sup>e</sup>, J. Smallcombe<sup>b</sup>, I.J. Thompson<sup>h</sup>, C. Waterfield<sup>a</sup>

<sup>a</sup> Astronomy and Physics Department, Saint Mary's University, Halifax, NS, B3H 3C3, Canada

<sup>b</sup> TRIUMF, Vancouver, BC, V6T 2A3, Canada

<sup>c</sup> Department of Chemistry, Simon Fraser University, Burnaby, BC, V5A 1S6, Canada

<sup>d</sup> Department of Physics, Simon Fraser University, Burnaby, BC, V5A 1S6, Canada

<sup>e</sup> Department of Physics and Astronomy, McMaster University, Hamilton, ON, L8S 4M1, Canada

<sup>f</sup> High Energy Accelerator Research Organization (KEK), Ibaraki 305-0801, Japan

<sup>g</sup> Lawrence Berkeley National Laboratory, Berkeley, CA 94720, USA

<sup>h</sup> Lawrence Livermore National Laboratory, P.O. Box 808, L-414, Livermore, CA 94551, USA

## ARTICLE INFO

Editor: B. Blank

## Keywords:

Neutron-rich nuclei  
Transfer reaction  
Inverse kinematics  
Shell structure  
Excited states

## ABSTRACT

A measurement of the excitation spectrum of  $^{94}\text{Kr}$  via one-neutron transfer to the ground state of  $^{93}\text{Kr}$  using the  $^{93}\text{Kr}(d,p)^{94}\text{Kr}$  reaction at 8A MeV, observing the outgoing protons, performed with the IRIS facility at TRIUMF is reported. Two states in  $^{94}\text{Kr}$ , at  $1.50\pm 0.14$  MeV and  $2.20\pm 0.14$  MeV, were observed. An adiabatic-wave approximation analysis of the differential cross sections leads us to identify the lower energy state as being populated with neutron transfer to the  $3s_{1/2}$  orbital. This leads to the first observation of the lowest  $0^+$  excited state in  $^{94}\text{Kr}$ , hence signaling shape co-existence. Theoretical calculations performed within the in-medium similarity renormalization group framework are presented that also show the existence of a low-energy  $0^+$  state, aligning qualitatively with the observation.

Regions of the nuclear chart where nuclear shape coexistence has been experimentally observed provide a rich testing ground for constraining theoretical models and better understanding the underlying effective interactions. The neutron-rich nuclei in the region of  $N = 50 - 60$  exhibit interesting evolution of nuclear shapes and shape coexistence. A sub-shell closure at  $N = 56$  is prominent in  $^{96}\text{Zr}$  [1–3] with high excitation energy of the first excited state. At  $N = 60$  a sudden large deformation emerges as reflected in the large  $B(E2)$  values for  $^{98}\text{Sr}$  and  $^{100}\text{Zr}$  and the increasing ratio of the energies of the  $4^+$  and  $2^+$  states, namely  $E(4^+)/E(2^+)$ . The Kr isotopes, however, show some interesting changes compared to the Sr and Zr isotopes. The  $E(4^+)/E(2^+)$  ratio is found to decrease for  $^{90-96}\text{Kr}$  in the region of  $N = 54 - 60$ . This could point to diminished collectivity in the Kr isotopes. Shell model calculations discuss the cause of the abrupt onset of deformation at  $N = 60$  in Zr isotopes to be due to the Type-II shell evolution [4]. These calcu-

lations show that the first excited  $0^+$  state changes shape continuously from a spherical configuration in the  $N = 50$  closed shell nucleus  $^{90}\text{Zr}$ , to an oblate shape in the  $N = 60$  nucleus  $^{96}\text{Zr}$  with the nuclei between them having triaxial and prolate shapes. The measured energies of the  $0^+$  states steeply decrease beyond the  $N = 50$  shell closure in Zr and Sr isotopes.

The presence of low-energy  $0^+$  excited states signals shape coexistence [5]. The  $0^+_{2,3}$  states at energies of 1.229 MeV and 1.465 MeV, respectively, in  $^{96}\text{Sr}$  ( $N = 58$ ) have been found to manifest shape coexistence. Analysis of the  $^{95}\text{Sr}(d,p)^{96}\text{Sr}$  reaction determined the  $3s_{1/2}$  spectroscopic factors for the ground state to be 0.19(3) and that for the excited  $0^+_2$  and  $0^+_3$  states were 0.22(3) and 0.33(13), respectively [6]. The ground state of  $^{95}\text{Sr}$  being dominated by the  $3s_{1/2}$  orbital, this reaction had a greater sensitivity to populate the spherical component of the  $0^+$  states, which was found to be higher for the excited states.

\* Corresponding author.

E-mail address: [ritu@triumf.ca](mailto:ritu@triumf.ca) (R. Kanungo).

<https://doi.org/10.1016/j.physletb.2025.139352>

Received 29 June 2024; Received in revised form 22 February 2025; Accepted 24 February 2025

There is very limited information on this  $0_2^+$  excited state in the Kr isotopes. The  $0_2^+$  state in  $^{88}\text{Kr}$  is similar to that of the  $N = 50$  closed shell isotope  $^{86}\text{Kr}$ , showing a deviation in the decreasing trend seen in Sr and Zr as well as from the theory predictions. This raises questions regarding shell evolution in the Kr isotopes. Theoretical predictions on the  $0_2^+$  state in the Kr isotopes are conflicting. Predictions in the interacting boson model (IBM-2) [7] show a gradual increase in the excitation energy of the  $0_2^+$  state beyond  $^{88}\text{Kr}$ , with the  $2_1^+$  state placed below it in all isotopes from  $N = 50 - 60$ . Contrary to this, the predictions in Ref. [8] using the symmetry-conserving configuration mixing method show progressive decrease in the  $0_2^+$  energies from  $^{88-94}\text{Kr}$  followed by an increase at  $N = 60$  in  $^{96}\text{Kr}$ .

The first excited state in  $^{94}\text{Kr}$  at 661.1(13) keV was initially observed using Coulomb excitation [7]. In later studies, the spontaneous fission of  $^{248}\text{Cm}$  [9] was used to populate excited states in  $^{94}\text{Kr}$ . Based on the observed gamma transitions in Ref. [9], the first excited  $2^+$  state at 665 keV and a  $4^+$  excited state at 1519 keV were considered to constitute the ground state band. The spins were determined from the angular correlation of the gamma rays. Recently, an isomeric state with a half-life of 32(3) ns in  $^{94}\text{Kr}$  was observed in the neutron induced fission of  $^{238}\text{U}$  and postulated to have a high spin of  $9^-$  [10]. In a recent study at the RIKEN RIBF, the excited states in  $^{94}\text{Kr}$  were populated using the  $^{95}\text{Kr}(p, pn)^{94}\text{Kr}$  knockout and  $^{94}\text{Kr}(p, p')^{\text{inelastic}}$  scattering reactions [11]. In addition to the known gamma transitions from the previous works, three new transitions were observed at 428(7) keV,  $880^{+22}_{-17}$  keV and  $1083^{+29}_{-27}$  keV that showed increased intensities when gated on the  $2_1^+ \rightarrow 0_{gs}^+$  gamma transition. These transitions however could not be placed in the level scheme presented in Ref. [11]. The level scheme postulates a possible spin of  $0^+$  or  $2^+$  for the lowest level above the  $2_1^+$  state, at 1.217 MeV.

An investigation of the low-energy excitation spectrum and a search to identify the  $0_2^+$  state in  $^{94}\text{Kr}$  ( $N = 58$ ) therefore can provide the first information on the existence or the absence of possible shape coexisting  $0^+$  states. It will also enable distinguishing between the different model predictions. Since the ground state spin of  $^{93}\text{Kr}$  is  $1/2^+$  [12], the  $(d, p)$  reaction selectively populates the  $0^+$  and  $2^+$  state(s) with  $L = 0$  and 2 angular momentum transfers, respectively.

The experiment was performed at the IRIS [13] reaction spectroscopy facility at the ISAC II radioactive beam facility [14] at TRIUMF. The  $^{93}\text{Kr}$  beam was produced from fission of a UC target induced by 480 MeV protons from the TRIUMF cyclotron.  $^{93}\text{Kr}$  ions were extracted using a FEBIAD ion source [15]. The beam of  $^{93}\text{Kr}$  was post-accelerated using the superconducting LINAC to 8A MeV and impinged on a solid deuterium target at IRIS. The average beam intensity of  $^{93}\text{Kr}$  at the reaction target was 200 pps. A schematic of the experimental setup is shown in Fig. 1. The protons from the  $^{93}\text{Kr}(d, p)$  reaction are detected by both the upstream and downstream detector arrays. The upstream detectors consist of two annular silicon strip arrays of 500  $\mu\text{m}$  thickness. The S3 type detector with 24 rings and 32 azimuthal sectors covered  $\theta_{lab} = 161^\circ - 174^\circ$  and the YY1 type detectors with eight azimuthal sectors and 16 rings in each covered  $\theta_{lab} = 122^\circ - 150^\circ$ . The downstream detectors are annular arrays of two layers forming an energy-loss ( $\Delta E$ ) and total energy (E) particle identification telescope. The first layer is a YY1 silicon strip detector array with thickness of 100  $\mu\text{m}$  with 8 azimuthal sectors, each of which is segmented into 16 rings. This is followed by the second layer, a CsI(Tl) array of thickness 12 mm consisting of 16 azimuthal sectors. They covered  $\theta_{lab} = 29^\circ - 55^\circ$ . Furthest downstream of the reaction target is an additional S3 type double-sided annular silicon detector. This is followed by a square double-sided silicon strip detector (DSSD) placed at zero degrees behind it. These detectors are sufficiently thick to stop the scattered beam particles.

The contaminants in the incoming beam were identified using their energy loss in an ionization chamber (IC) upstream of the reaction target, which was filled with isobutane gas at 19.5 Torr. The energy-loss spectrum from the IC is shown in Fig. 2, where  $^{93}\text{Kr}$  is seen to be the dominant component. A majority of the contaminants originate from

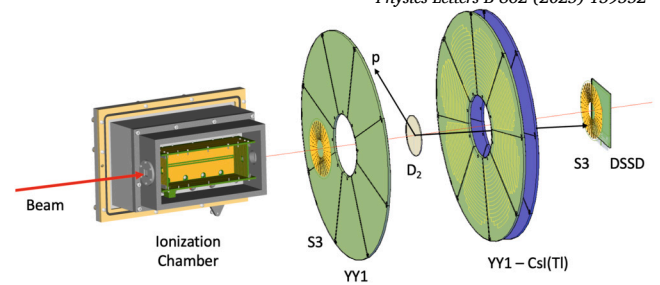


Fig. 1. Experimental setup showing the detectors used in the experiment. YY1 detectors are single-sided segmented silicon strip detector array, S3 detectors are annular double sided segmented silicon strip detectors. The DSSD detector is a double sided square silicon strip detector. Beam is coming from left to right.

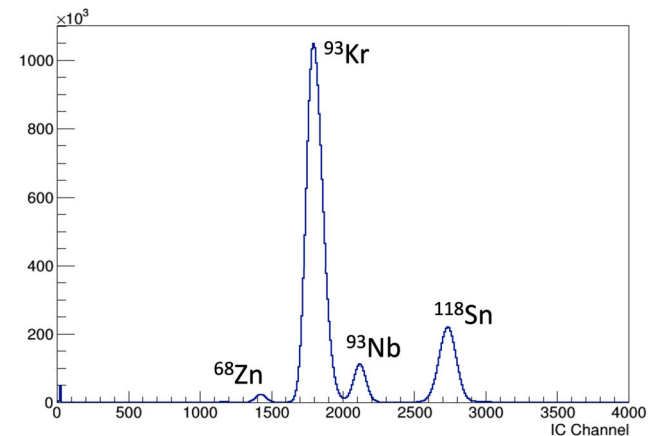
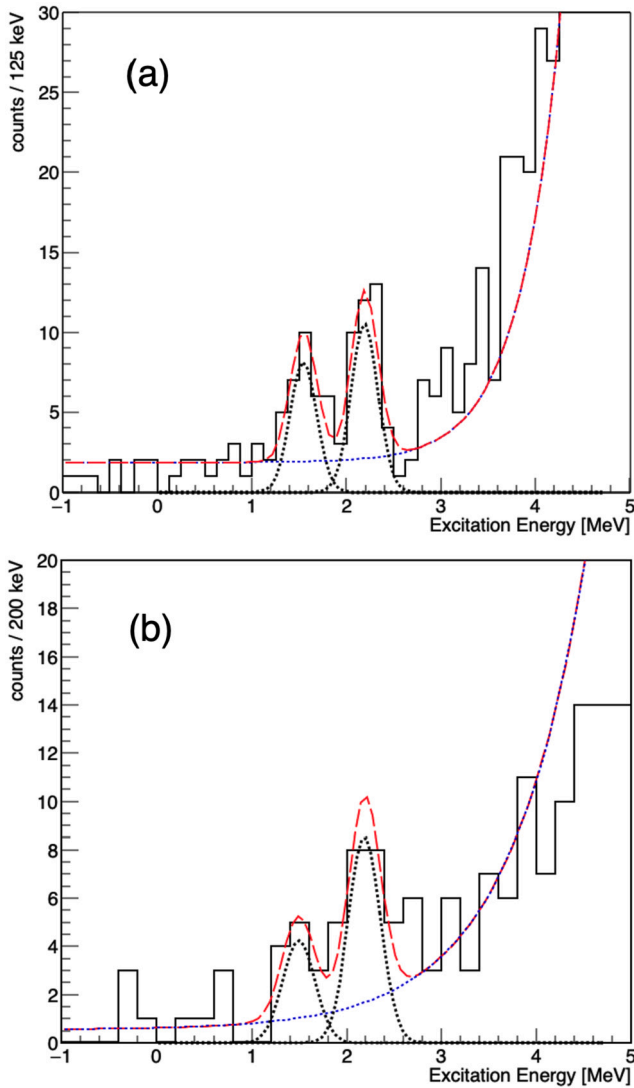


Fig. 2. Ionization chamber spectrum showing the different incoming beam species observed in the experiment, as labeled.

the ECRIS charge breeder [16] that was used for charge breeding  $^{93}\text{Kr}$  to make it suitable for post-acceleration.

The solid  $\text{D}_2$  target has a copper target cell with a circular aperture of diameter 5 mm which is the area of the  $\text{D}_2$  target. The cell is backed by a thin (4.33  $\mu\text{m}$ ) silver (Ag) foil. The target cell is connected to a cold-head held at a temperature around 4 K. The solid deuterium target is formed using a  $\text{D}_2$  gas diffuser that is sprayed onto the cold Ag foil. The accelerated beam is transmitted through the aperture and through the Ag and  $\text{D}_2$  layers. The orientation of the target cell for this measurement was set with the deuterium target layer faced upstream. This creates a window-less target condition, such that the low-energy protons emitted from the  $(d, p)$  reaction reach the upstream detectors without passing through any other material. The average target thickness was  $\sim 50 \mu\text{m}$  and was determined from the difference in the energy of the beam particle with and without the  $\text{D}_2$  target measured using the end silicon DSSD detector.

The kinematics of reaction channels emitting  $d$ ,  $t$ , and He nuclei dictate that they emerge only in the forward laboratory angles, while the  $(d, p)$  reaction emits protons in the backward and forward laboratory angles. The  $\theta_{lab} > 90^\circ$  for the  $(d, p)$  correspond to forward center of mass angles. To reduce background events, an event-by-event analysis therefore required coincidence between the detection of backwards scattered protons in the upstream silicon detector array, and the detection of Kr nuclei in the zero degree DSSD placed downstream of the target. The background originating from reactions from the Ag foil was measured by evaporating the solid deuterium target. The maximum likelihood method was used to extract a fit to the background data as well as estimate the uncertainty in the fit. The normalization of counts in the ion chamber, gated by the  $^{93}\text{Kr}$  peak with and without the solid deuterium target was used to extract a scaling factor for the background subtraction from the Ag foil for the data with the  $\text{D}_2$  target. In the downstream



**Fig. 3.** Excitation spectra for  $^{94}\text{Kr}$  derived from the missing mass measurement showing the scaled background fit (blue), Gaussian fit to the two excited states (black dotted curve), and the total fit to the data (red curve). Panel (a) is extracted from the upstream YY1 detectors, panel (b) is from the downstream YY1-CsI(Tl) detectors.

detector telescope, the protons were identified using the energy-loss vs total energy ( $\Delta E$ -E) correlation method.

The missing mass technique was used to reconstruct the excitation spectrum of  $^{94}\text{Kr}$  using the measured energies and scattering angles of the protons detected in the upstream silicon detector array and the downstream  $\Delta E$ -E telescope. Fig. 3(a) shows the measured excitation spectrum for  $^{94}\text{Kr}$  derived from the missing mass measurement for the angles covered by the upstream detector array. The spectrum shows two prominent peaks at excitation energies of  $1.50 \pm 0.14$  MeV and  $2.20 \pm 0.14$  MeV. The scaled background (blue curves) was subtracted from the data in order to extract the differential cross sections for each excited state. Fig. 3(b) shows the  $^{94}\text{Kr}$  excitation spectrum reconstructed using the proton events detected in the downstream detector telescope, which covers larger center-of-mass angles. Two excited state peaks are observed at energies  $1.50 \pm 0.17$  MeV and  $2.20 \pm 0.17$  MeV, that are in agreement with those observed in the upstream detector.

The differential cross-sections were calculated using the Adiabatic Wave Approximation (ADWA) formalism, using the code TWOFNR [17]. The global optical parameters of Johnson and Tandy [18] and Koning-Delaroche (KD) [19] were used to generate the adiabatic potentials for

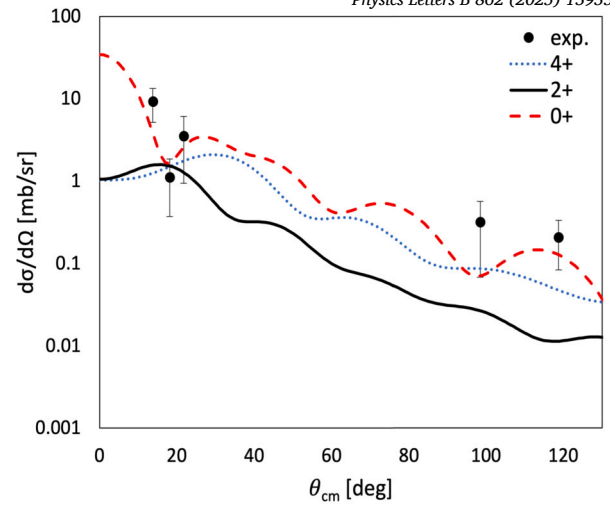


**Fig. 4.** Differential cross section data with statistical uncertainties (filled circles) for the excited state at 1.50 MeV. The ADWA calculation fits for a spin of  $0^+/2^+/4^+$  are shown by the dashed/solid/dotted curves.

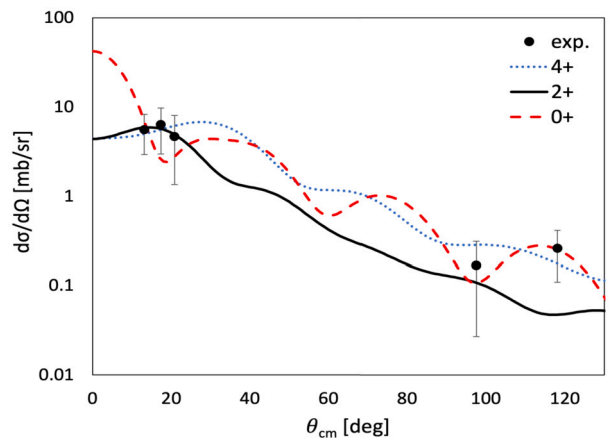


**Fig. 5.** Differential cross section data with statistical uncertainties (filled circles) for the excited state at 2.2 MeV. The ADWA calculation fits for a spin of  $0^+/2^+/4^+$  are shown by the dashed/solid/dotted curves.

each of the spin parity assignments explored in this study. Fig. 4 shows the comparison of the measured differential cross section from this work to ADWA theoretical predictions assuming different spin assignments for the excited state observed at 1.50 MeV.

The calculations with angular momentum transfer  $L = 0$ , yields the best fit with reduced  $\chi^2 \approx 1.2$  while those with  $L = 2$  and  $L = 4$  are both around 2.3. The  $\chi^2$  values for each fit were extracted using the least squares method, using only the small center of mass angles (first three data points) where the direct reaction mechanism allows extraction of  $L$  and the spectroscopic factor most reliably. Calculations within the distorted wave Born approximation (DWBA) were also performed as a confirmation of the results using the code FRESKO [20], which resulted in the same  $L = 0$  for best fit and is therefore not shown in Fig. 4. This leads to the inference that the state observed at 1.50 MeV has a spin of  $0^+$  arising from the transfer of a neutron to the  $3s_{1/2}$  orbital. Moreover, the  $(d,p)$  transfer reaction has strong selectivity to populating the  $0^+$  state(s) from  $L = 0$  transfer and  $2^+$  state(s) from  $L = 2$  transfer. Population of a  $4^+$  state would require  $L = 4$  transfer and is therefore suppressed. Therefore, the observed state at 1.5 MeV populated in this  $(d,p)$  transfer reaction is a new  $0^+$  excited state. The normalization factor of the calculation provides the spectroscopic factor of  $2.14 \pm 0.82$ , where the uncertainty in the normalization factor takes into account both the

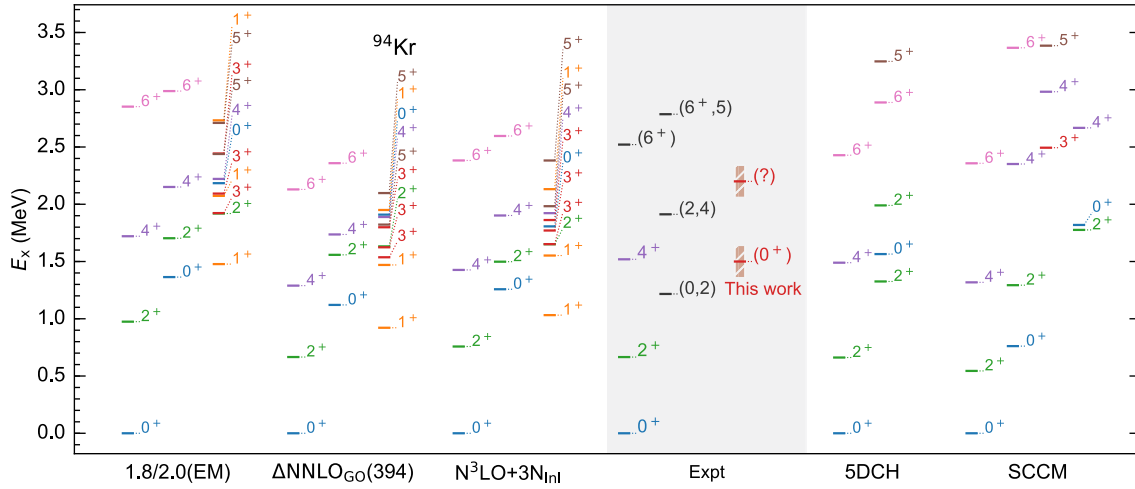


Fig. 6. IMSRG predictions of excited states in  $^{94}\text{Kr}$  with the three chiral interactions (see text). The experimental data are shown in the shaded band region. Comparison to predictions of 5DCH Ref. [11] and SCCM Ref. [8] models are shown.

statistical as well as the systematic uncertainties. The uncertainty of the target thickness is  $\pm 10\%$  which leads to the systematic uncertainty. The large  $s$  orbital  $L = 0$  strength for the state indicates that it has a strong spherical component. In contrast the  $^{94}\text{Kr}_{gs}(0^+)$  was not observed, i.e. not appreciably populated, in the addition of neutron to the ground state of  $^{93}\text{Kr}$ , via the  $(d, p)$  reaction. This shows that the ground state of  $^{94}\text{Kr}$  has likely a stronger deformed component. From the non-observation of the  $^{94}\text{Kr}_{gs}$ , an upper limit of the spectroscopic factor for the  $3s_{1/2}$  orbital is deduced to be 0.25.

Fig. 5 shows the comparison of the measured differential cross section for the observed excited state at 2.20 MeV to ADWA theoretical predictions for different spin assignments. The data can be described by either  $L = 2$  or  $L = 4$  that result in reduced  $\chi^2$  values of 0.025 and 0.15, respectively while that for  $L = 0$  is 0.91. Therefore, we do not make any definitive spin assignment for this state. The normalization factor for the calculation to reproduce the data for  $L = 2$  transfer to the  $2d_{3/2}$  orbital is  $0.3 \pm 0.1$  while that for  $L = 4$  to the  $1g_{7/2}$  orbital is  $2.6 \pm 0.8$ . A comparison to DWBA predictions using FRESKO was also performed for the 2.2 MeV excited state resulting in the same description of either  $L = 2$  or  $L = 4$  of the data. The data for the 1.5 MeV state (2.2 MeV state) has a statistical uncertainty of 37% (35%) in the forward center of mass angles and a systematic uncertainty of 10% from target thickness. This leads to an uncertainty in the spectroscopic factor of 38% (36%) for the 1.5 MeV (2.2 MeV) state.

We compare (Fig. 6) the experimental data with *ab initio* valence-space in-medium similarity renormalization group (VS-IMSRG) calculations [21–23] based on three different chiral two- (NN) and three-nucleon (3N) interactions, 1.8/2.0(EM) [24,25],  $\text{N}^3\text{LO}+3\text{N}_{\text{inl}}$  [26], and  $\Delta\text{NNLO}_{\text{GO}}$  [27]. The 1.8/2.0(EM) and  $\text{N}^3\text{LO}+3\text{N}_{\text{inl}}$  interactions, while only fit to  $A \leq 4$  data, generally reproduce ground-state energies across the light to the heavy-mass regions [26,28,29]. In contrast,  $\Delta\text{NNLO}_{\text{GO}}$  includes explicit  $\Delta$ -isobar degrees of freedom and optimizes NN and 3N forces simultaneously at the  $\text{N}^2\text{LO}$  level. Working in an initial harmonic-oscillator basis of 15 major shells at a frequency of 16 MeV, we impose an additional cut on 3N force matrix elements storage  $E_{3\text{max}} = 24$  [30]. We first transform to the Hartree-Fock basis, then use the VS-IMSRG [21,22,31] to construct approximate unitary transformations to decouple a core and valence-space Hamiltonian from the full  $A$ -body Hamiltonian. In this work, we employ the  $^{78}\text{Ni}$  core with a  $\pi p f_{5/2}$  and  $\nu s d g_{7/2}$  valence space, where the final exact diagonalization was performed using the KSHELL shell-model code [32].

It is interesting to note that the IMSRG calculations predict a low-energy  $0_2^+$  excited state above the first  $2_1^+$  state (Fig. 6). The  $\Delta\text{NNLO}_{\text{GO}}$  and the  $\text{N}^3\text{LO}+3\text{N}_{\text{inl}}$  interactions predict the  $0_2^+$  state to be just below the

$4_1^+$  state. This predicted level likely aligns with the observed 1.50 MeV state inferred as a  $0^+$  excited state in this work. The calculated spectroscopic factors for overlap of the  $^{93}\text{Kr}_{gs}$  and the  $^{94}\text{Kr}_{gs}(^{94}\text{Kr}(0_2^+))$  states, with neutrons in the  $3s_{1/2}$  orbital, are 0.94(0.41) with the 1.8/2.0(EM) interaction, 0.54(0.45) with the  $\Delta\text{NNLO}_{\text{GO}}$  interaction and 0.70(0.39) with the  $\text{N}^3\text{LO}+3\text{N}_{\text{inl}}$  interaction. It is seen that the  $\Delta\text{NNLO}_{\text{GO}}$  interaction that predicts a much smaller spherical component for the  $^{94}\text{Kr}_{gs}$  also has the energy of the  $2^+$  first excited state in best agreement with the experiment.

The proton-neutron interacting boson model (IBM-2) [7] uses monopole and quadrupole bosons that are associated with the collective  $J^\pi = 0^+$  and  $2^+$  proton or neutron valence pairs, respectively. These calculations adopted the Gogny D1M energy density functional. Ref. [8] is based on the generator coordinate method using the Symmetry Conserving Configuration Mixing (SCCM) that includes mixing of axial and triaxial energy states. The prediction of the  $0_2^+$  state in Ref. [8] is around 0.75 MeV while that in Ref. [7] is around 2.75 MeV. The observed energy of  $1.50 \pm 0.14$  MeV lies between these predicted energies. The predicted  $0^+$  excited state energy from the five-dimensional collective Hamiltonian (5DCH) beyond-mean-field model [11] with Gogny D1M interaction however is in fairly close agreement with the observed state in this work. The difference in the predicted energies in Ref. [7] and Ref. [11], both using the Gogny D1M interaction, illustrates that the interaction used is not driving the variance.

The observed excited states do not coincide with the levels reported from gamma spectroscopy in Ref. [11]. However one may note that an observed  $\gamma$ -transition at 880 keV reported in Ref. [11], that is not included in the level scheme, was enhanced with the selection of the 665 keV  $\gamma$ -transition. A cascade decay of these two transitions would lead to an excitation energy of around 1.5 MeV.

The observation of the low-energy  $0^+$  state at 1.5 MeV signals shape coexistence in  $^{94}\text{Kr}$ . A possible scenario could be that the two excited states observed in this work at 1.50 MeV and 2.20 MeV might belong to an excited (spherical) band.

In summary, the first measurement of the  $^{93}\text{Kr}(d, p)^{94}\text{Kr}$  reaction reported here has revealed low-energy excited states observed at excitation energies  $1.50 \pm 0.14$  MeV and  $2.20 \pm 0.14$  MeV in  $^{94}\text{Kr}$ , while the ground state was not observed. An adiabatic-wave approximation analysis of the angular distributions of the states suggests the spin of the state at 1.50 MeV to be  $0^+$  populated with neutron transfer to the  $3s_{1/2}$  orbital. This could signal shape co-existence. *Ab initio* calculations in the IMSRG framework presented in this work also predict a low-energy  $0_2^+$  excited state. These findings call for new theoretical investigations to explain the observed states and further experimental investigations to

determine the spins of the higher excited states and a possible spherical band structure. In the future, availability of more than two orders of magnitude higher beam intensity of  $^{94}\text{Kr}$  would allow  $\gamma$  spectroscopy measurements, such as ( $d, p\gamma$ ), to determine the level scheme for the decay of the  $0_2^+$  state.

### Declaration of competing interest

The authors declare that they have no known competing financial interests or personal relationships that could have appeared to influence the work reported in this paper.

### Acknowledgements

The authors thank the TRIUMF ISAC beam delivery team and the cyclotron operations team. The support from NSERC, Canada Foundation for Innovation and Nova Scotia Research and Innovation Trust is gratefully acknowledged. TRIUMF receives funding via a contribution through the National Research Council Canada. The support from RCNP for the target is gratefully acknowledged. It was partly supported by the grant-in-aid program of the Japanese government under the contract number 23224008 and 14J03935.

### Data availability

Data relevant to the results published in this work can be made available upon reasonable request to the corresponding author.

### References

- [1] G. Molnár, T. Belgya, A. Verbs, S. Yates, E. Kleppinger, R. Gatenby, R. Julin, J. Kumpulainen, A. Passoja, E. Verho, Particle-hole and vibrational states in doubly closed subshell  $^{96}\text{Zr}$  from in-beam inelastic neutron and proton scattering, *Nucl. Phys. A* 500 (1989) 43–76.
- [2] H. Mach, G. Molnár, S.W. Yates, R.L. Gill, A. Aprahamian, R.A. Meyer, Intruder state collectivity at a double subshell closure from the beta decay of  $0^-$   $^{96}\text{Zr}$  to the levels of  $^{96}\text{Zr}$ , *Phys. Rev. C* 37 (1988) 254.
- [3] I. Boboshin, V. Varlamov, B. Ishkhanov, E. Romanovsky, New double-magic nucleus  $^{96}\text{Zr}$  and conditions for existence of new magic nuclei, *Phys. At. Nucl.* 70 (2007) 1363.
- [4] T. Togashi, Y. Tsunoda, T. Otsuka, N. Shimizu, Quantum phase transition in the shape of Zr isotopes, *Phys. Rev. Lett.* 117 (2016) 172502.
- [5] P.E. Garrett, M. Zeilińska, E. Clément, An experimental view on shape coexistence in nuclei, *Prog. Part. Nucl. Phys.* 124 (2022) 103931, <https://doi.org/10.1016/j.pnpnp.2021.103931>.
- [6] S. Cruz, P. Bender, R. Krücken, K. Wimmer, F. Ames, C. Andreoiu, R. Austion, C. Bancroft, R. Braid, T. Bruhn, W. Catford, A. Garnsworthy, G. Hackman, R. Kanungo, A. Knapton, W. Kortem, K. Kuhn, J. Lassen, M. Laxdal, R. Marchetto, A. Matta, D. Miller, M. Moukaddam, N. Orr, N. Sachmpazidi, A. Sanetullaev, C. Svensson, N. Terpstra, C. Unsworth, P. Voss, Shape coexistence and mixing of low-lying  $0^+$  states in  $^{96}\text{sr}$ , *Phys. Lett. B* 786 (2018) 94, <https://doi.org/10.1016/j.physletb.2018.09.031>.
- [7] M. Albers, N. Warr, K. Nomura, A. Blazhev, J. Jolie, D. Mücher, B. Bastin, C. Bauer, C. Bernards, L. Bettermann, V. Bildstein, J. Butterworth, M. Cappellazzo, J. Ced-erkäll, D. Cline, I. Darby, S. Das Gupta, J.M. Daugas, T. Davinson, H. De Witte, J. Diriken, D. Filipescu, E. Fiori, C. Fransen, L.P. Gaffney, G. Georgiev, R. Gernhäuser, M. Hackstein, S. Heinze, H. Hess, M. Huysse, D. Jenkins, J. Konki, M. Kowalczyk, T. Kröll, R. Krücken, J. Litzinger, R. Lutter, N. Marginean, C. Mihai, K. Moschner, P. Napiorkowski, B.S. Nara Singh, K. Nowak, T. Otsuka, J. Pakarinen, M. Pfeiffer, D. Radeck, P. Reiter, S. Rigby, L.M. Robledo, R. Rodríguez-Guzmán, M. Rudigier, P. Sarriguren, M. Scheck, M. Seidlitz, B. Siebeck, G. Simpson, P. Thöle, T. Thomas, J. Van de Walle, P. Van Duppen, M. Vermeulen, D. Voulot, R. Wadsworth, F. Wenander, K. Wimmer, K.O. Zell, M. Zielinska, Evidence for a smooth onset of deformation in the neutron-rich Kr isotopes, *Phys. Rev. Lett.* 108 (2012) 062701, <https://doi.org/10.1103/PhysRevLett.108.062701>.
- [8] T. Rodríguez, Structure of krypton isotopes calculated with symmetry-conserving configuration-mixing methods, *Phys. Rev. C* 90 (2014) 034306.
- [9] T. Rzaca-Urban, W. Urban, A. Kaczor, J. Durell, M. Leddy, M. Jones, W. Phillips, A. Smith, B. Varley, I. Ahmad, L. Morss, M. Benteleb, E. Lubkiewicz, N. Schulz, Shapes of the neutron-rich  $^{88-94}\text{Kr}$  nuclei, *Eur. Phys. J. A* 9 (2000) 165.
- [10] R.-B. Gerst, A. Blazhev, N. Warr, J.N. Wilson, M. Lebois, N. Jovančević, D. Thisse, R. Canavan, M. Rudigier, D. Étasse, E. Adamska, P. Adsley, A. Algora, M. Babo, K. Belvedere, J. Benito, G. Benzioni, A. Boso, S. Bottoni, M. Bunce, R. Chakma, N. Cieplicka-Oryńczak, S. Courtin, M.L. Cortés, P. Davies, M. Delafosse, C. Fallot, B. Fomal, L.M. Fraile, D. Gjestvang, A. Gottardo, V. Guadilla, G. Häfner, K. Hauschild, M. Heine, C. Henrich, I. Homm, F. Ibrahim, W. Iskra, P. Ivanov, S. Jazrawi, A. Korgul, P. Koseoglou, T. Kröll, T. Kurtukian-Nieto, L. Le Meur, S. Leoni, J. Ljungvall, A. Lopez-Martens, R. Lozeva, I. Matea, K. Miernik, J. Nemer, S. Oberstedt, W. Paulsen, M. Piersa, Y. Popovitch, C. Porzio, L. Qi, D. Ralet, P.H. Regan, D. Reygadas-Tello, K. Rezykina, V. Sánchez-Tembleque, C. Schmitt, P.-A. Söderström, C. Sürder, G. Tocabens, V. Vedia, D. Verney, B. Wasilewska, J. Wiederhold, M. Yavachova, F. Zeiser, S. Ziliani, Prompt and delayed  $\gamma$  spectroscopy of neutron-rich  $^{94}\text{kr}$  and observation of a new isomer, *Phys. Rev. C* 102 (2020) 064323, <https://doi.org/10.1103/PhysRevC.102.064323>.
- [11] R.-B. Gerst, A. Blazhev, K. Moschner, P. Doornenbal, A. Obertelli, K. Nomura, J.-P. Ebran, S. Hilaire, J. Libert, G. Authalet, H. Baba, D. Calvet, F. Château, S. Chen, A. Corsi, A. Delbart, J.-M. Gheller, A. Giganon, A. Gillibert, V. Lapoux, T. Motobayashi, M. Niikura, N. Paul, J.-Y. Roussé, H. Sakurai, C. Santamaria, D. Steppenbeck, R. Taniuchi, T. Uesaka, T. Ando, T. Arici, F. Browne, A.M. Bruce, R. Caroll, L.X. Chung, M.L. Cortés, M. Dewald, B. Ding, F. Flavigny, S. Franchoo, M. Górska, A. Gottardo, J. Jolie, A. Jungclaus, J. Lee, M. Lettmann, B.D. Linh, J. Liu, Z. Liu, C. Lizarazo, S. Momiya, S. Nagamine, N. Nakatsuka, C.R. Nita, C. Nobs, L. Olivier, R. Orlandi, Z. Patel, Z. Podolyák, M. Rudigier, T. Saito, C. Shand, P.-A. Söderström, I. Stefan, V. Vaquero, V. Werner, K. Wimmer, Z. Xu,  $\gamma$ -ray spectroscopy of low-lying yrast and non-yrast states in neutron-rich  $^{94,95,96}\text{kr}$ , *Phys. Rev. C* 105 (2022) 024302, <https://doi.org/10.1103/PhysRevC.105.024302>.
- [12] M. Keim, E. Arnold, W. Borchers, U. Georg, A. Klein, R. Neugart, L. Vermeeren, R.E. Silverans, P. Lievens, Laser spectroscopy measurements of  $^{72-96}\text{Kr}$  spins, moments and charge radii, *Nucl. Phys. A* 586 (1995) 219.
- [13] R. Kanungo, Iris: the ISAC charged particle reaction spectroscopy facility for reaccelerated high-energy ISOL beams, *Hyperfine Interact.* 225 (2014) 235, <https://doi.org/10.1007/s10751-013-0904-8>.
- [14] J. Dilling, R. Krücken, G. Ball, ISAC Overv. 225 (2014) 1, <https://doi.org/10.1007/s10751-013-0877-7>.
- [15] P.G. Bricault, F. Ames, M. Domsbky, P. Kunz, J. Lassen, *Hyperfine Interact.* 225 (2014) 25.
- [16] F. Ames, R. Baartman, K. Jayamanna, *Hyperfine Interact.* 225 (2014) 63.
- [17] J. Tostevin, University of surrey version of the code *TWOFNR* (of M. Toyama, M. Igarashi and N. Kishida) and code front, private communication (2014).
- [18] R. Johnson, P. Tandy, An approximate three-body theory of deuteron stripping, *Nucl. Phys. A* 235 (1) (1974) 56–74.
- [19] A. Koning, J. Delaroche, Local and global nucleon optical models from 1 keV to 200 MeV, *Nucl. Phys. A* 713 (3) (2003) 231–310.
- [20] I.J. Thompson, Coupled reaction channels calculations in nuclear physics, *Comput. Phys. Rep.* 7 (4) (1988) 167–212.
- [21] S.R. Stroberg, A. Calci, H. Hergert, J.D. Holt, S.K. Bogner, R. Roth, A. Schwenk, Nucleus-dependent valence-space approach to nuclear structure, *Phys. Rev. Lett.* 118 (2017) 032502, <https://doi.org/10.1103/PhysRevLett.118.032502>, <https://link.aps.org/doi/10.1103/PhysRevLett.118.032502>.
- [22] S.R. Stroberg, S.K. Bogner, H. Hergert, J.D. Holt, Non-empirical interactions for the nuclear shell model: an update, *Annu. Rev. Nucl. Part. Sci.* 69 (2019) 307–362, <https://doi.org/10.1146/annurev-nucl-101917-021120>.
- [23] B. Hu, W. Jiang, T. Miyagi, Z. Sun, A. Ekström, C. Forssén, G. Hagen, J.D. Holt, T. Papenbrock, S.R. Stroberg, I. Vernon, Ab initio predictions link the neutron skin of  $^{208}\text{Pb}$  to nuclear forces, *Nat. Phys.* 18 (10) (2022) 1196, <https://doi.org/10.1038/s41567-022-01715-8>.
- [24] K. Hebel, S.K. Bogner, R.J. Furnstahl, A. Nogga, A. Schwenk, Improved nuclear matter calculations from chiral low-momentum interactions, *Phys. Rev. C* 83 (2011) 031301(R), <https://doi.org/10.1103/PhysRevC.83.031301>, <https://link.aps.org/doi/10.1103/PhysRevC.83.031301>.
- [25] J. Simonis, S.R. Stroberg, K. Hebel, J.D. Holt, A. Schwenk, Saturation with chiral interactions and consequences for finite nuclei, *Phys. Rev. C* 96 (2017) 014303, <https://doi.org/10.1103/PhysRevC.96.014303>, <https://link.aps.org/doi/10.1103/PhysRevC.96.014303>.
- [26] V. Somà, P. Navrátil, F. Raimondi, C. Barbieri, T. Duguet, Novel chiral Hamiltonian and observables in light and medium-mass nuclei, *Phys. Rev. C* 101 (2020) 014318, <https://doi.org/10.1103/PhysRevC.101.014318>, <https://link.aps.org/doi/10.1103/PhysRevC.101.014318>.
- [27] W.G. Jiang, A. Ekström, C. Forssén, G. Hagen, G.R. Jansen, T. Papenbrock, Accurate bulk properties of nuclei from  $A = 2$  to  $\infty$  from potentials with  $\Delta$  isobars, *Phys. Rev. C* 102 (2020) 054301, <https://doi.org/10.1103/PhysRevC.102.054301>, <https://link.aps.org/doi/10.1103/PhysRevC.102.054301>.
- [28] T.D. Morris, J. Simonis, S.R. Stroberg, C. Stumpf, G. Hagen, J.D. Holt, G.R. Jansen, T. Papenbrock, R. Roth, A. Schwenk, Structure of the lightest tin isotopes, *Phys. Rev. Lett.* 120 (2018) 152503, <https://doi.org/10.1103/PhysRevLett.120.152503>, <https://link.aps.org/doi/10.1103/PhysRevLett.120.152503>.
- [29] S.R. Stroberg, J.D. Holt, A. Schwenk, J. Simonis, Ab initio limits of atomic nuclei, *Phys. Rev. Lett.* 126 (2) (2021) 022501, <https://doi.org/10.1103/PhysRevLett.126.022501>.
- [30] T. Miyagi, S.R. Stroberg, P. Navrátil, K. Hebel, J.D. Holt, Converged ab initio calculations of heavy nuclei, *Phys. Rev. C* 105 (2022) 014302, <https://doi.org/10.1103/PhysRevC.105.014302>, <https://link.aps.org/doi/10.1103/PhysRevC.105.014302>.

- [31] T. Miyagi, S.R. Stroberg, J.D. Holt, N. Shimizu, Ab initio multishell valence-space Hamiltonians and the island of inversion, *Phys. Rev. C* 102 (2020) 034320, <https://doi.org/10.1103/PhysRevC.102.034320>, <https://link.aps.org/doi/10.1103/PhysRevC.102.034320>.
- [32] N. Shimizu, T. Mizusaki, Y. Utsuno, Y. Tsunoda, Thick-restart block Lanczos method for large-scale shell-model calculations, *Comput. Phys. Commun.* 244 (2019) 372, <https://doi.org/10.1016/j.cpc.2019.06.011>, <http://www.sciencedirect.com/science/article/pii/S0010465519301985>.